JCTC Journal of Chemical Theory and Computation

Article

pubs.acs.org/JCTC

# Generalization of Natural Bond Orbital Analysis to Periodic Systems: Applications to Solids and Surfaces via Plane-Wave Density Functional Theory

Benjamin D. Dunnington and J. R. Schmidt*

Department of Chemistry and Theoretical Chemistry Institute, University of Wisconsin—Madison, 1101 University Avenue, Madison, Wisconsin 53706, United States

**ABSTRACT:** Natural bond orbital (NBO) analysis is a powerful analysis technique capable of generating intuitive chemical representations of otherwise complex quantum mechanical electronic structure results, yielding a localized "Lewis-like" description of bonding and reactivity. We generalize this algorithm to periodic systems, thus expanding the scope of NBO analysis to bulk materials and/or periodic surface models. We employ a projection scheme to further expand the algorithm's applicability to ubiquitous plane-wave density functional theory (PW DFT) calculations. We also present a variety of example applications: examining bulk bonding and surface reconstruction and elucidating fundamental aspects of heterogeneous catalysis—all derived from rigorous underlying PW DFT calculations.

## I. INTRODUCTION

Natural bond orbital (NBO) analysis[1−4] has proven to be an invaluable tool, facilitating the interpretation of electronic structure calculations in a chemically intuitive manner. NBO analysis replaces the delocalized canonical molecular orbitals with a set of transferable[5] localized bonding orbitals and lone pairs, with a strong connection to the ubiquitous Lewis structures of general chemistry. The analysis is "natural" since it is based solely on the density matrix, obtained from the underlying electronic structure calculation. This lack of artificial parameters helps ensure robust, physically motivated results and chemical insights into bonding and reactivity.

NBO has already proven capable of interpreting complex bonding and reactivity in *molecular* systems.[6−15] Via a series of methodological developments, the present work seeks to extend the basic NBO approach to analyze bonding in periodic solid state systems and surface models. The latter case is particularly compelling in that it opens the door to NBO-based studies of heterogeneously catalyzed reactions,[14,15] with potential impact in areas such as biomass conversion, involving the decomposition and/or reforming of complex organic molecules.[16−18] Note that the NBO approach was recently extended to deal with the case of multicenter two-electron bonding, yielding the adaptive natural density partitioning (AdNDP) scheme.[19] AdNDP has provided chemically interpretable representations of bonding in aromatic organic compounds,[20] transition metal complexes,[21,22] and metallic nanoparticles.[23]

Generalization of NBO or AdNDP to bulk (periodic) systems or surfaces has not previously been realized due to a variety of fundamental challenges. First, the most natural description of the electronic wave function for periodic systems is given in reciprocal space as per Bloch's theorem, naturally accounting for periodicity but yielding orbitals delocalized over all space.[24] In contrast, we seek a *localized*, real space representation and must thus expressly account for the periodicity of the system. Second, while there are widely available atomic orbital (AO)-based electronic structure packages for use on periodic systems, the majority of computational studies of solid state/surface systems utilize plane-wave (PW) density functional theory (DFT). Their periodic nature makes PWs a natural choice for solid state systems, and PW DFT offers an efficient methodology for studying periodic bulk and surface structures.[25,26] NBO analysis, however, requires a density matrix in a localized atom-centered basis set and will therefore require additional interfacing for application to delocalized PWs.

There are currently only a handful of computational analysis methods applicable to periodic systems that are compatible with both PWs and atom-centered basis sets, including maximally localized Wannier functions, crystal orbital Hamiltonian population analysis, and atoms-in-molecules.

Maximally localized Wannier functions[27,28] (MLWF) have been used to describe bonding in periodic systems, including those of catalytic relevance.[29−31] Here, the band structure is transformed to a set of functions localized within a single real space unit cell via Wannier transform. The resulting real space bands are then further transformed, *within* a unit cell, such that a particular localization metric is optimized, similar to the approach of localized molecular orbitals. However, the resulting MLWF orbitals are largely mathematical, especially in application to PW basis sets, and lack explicit hybridization information natural to chemical descriptions of bonding. Furthermore, this process is only rigorously defined for insulators, and treatment of other systems requires subtle manipulation of the band structure.[28] The approach does, however, provide a natural description of many-center bonding, allowing localization intrinsic to the system to be found. While most NBO implementations are limited to two- or three-centered bonds (although this limit is not intrinsic), NBO also provides an inherently chemical picture as the obtained local

**Received:** January 3, 2012
**Published:** May 3, 2012





dx.doi.org/10.1021/ct300002t | *J. Chem. Theory Comput.* 2012, 8, 1902−1911

orbitals are described as linear combinations of atom-centered hybrids.

Alternatively, the crystal orbital overlap population[32,33] (COOP) analysis of Hoffmann and Hughbanks was generalized from Hückel theory to DFT via the crystal orbital Hamiltonian population[34] (COHP) approach. COHP is based in reciprocal space and provides a *k*-point-dependent depiction of bonding. This has allowed for an inherently chemical understanding of materials properties that rely on delocalized interactions, such as crystal structure rationalization[33] and ferromagnetism.[35] Alternatively, NBO provides purely localized real space representations of bonding interactions. This would be preferable for studying interactions on a localized basis, such as adsorption onto a supported nanoparticle. Although COHP was previously limited to calculations involving tight binding basis sets, it has recently been extended to PW DFT via a projection technique.[36] (Note that this projection is rigorously limited to *orthonormal* atom-centered basis functions.)

Finally, the atoms-in-molecules (AIM) approach connects the topology of a system's electron density to notions of atoms and bonding and is equally applicable to both molecular and periodic systems.[37,38] AIM partitions space into atomic basins based on electron density. Scalar properties related to the density (e.g., atomic charge) can then be integrated over these basins and the resulting value assigned to the associated atomic center. The volumes defined by these basins have found use in many applications, rigorously dividing a molecule into its atomic components. Networks of bonding connections, including multicenter motifs, are generated by locating the critical points of the electron density. The AIM framework has been applied to an expansive range of systems, including analysis of the catalyst surface active sites and defect effects.[39,40] While AIM yields a connectivity graph in terms of the rigorous electron density that maps the complete bonding pattern, including noncovalent interactions, it can be difficult to identify underlying orbital interactions contributing to these connections. For example, in a molecule like ethylene, the carbon−carbon interaction is only identified as a "bond," without separate $\pi$- and $\sigma$-bonding contributions.[38] While the interatomic bonds found in NBO analyses are limited to largely covalent interactions, all bonds are obtained as explicitly orbital interactions. Additionally, noncovalent interactions can be probed using delocalization analysis within the NBO framework.[3]

The inherently chemical and localized nature of NBO poses it to provide a unique and chemically meaningful tool to analyze bonding in bulk materials and surfaces, complimenting these existing techniques. As such, we present here a generalization of the NBO approach to periodic electronic structure calculations. We first establish the theoretical underpinnings of the extension of NBO to periodic systems and then present the associated PW-to-AO projection algorithm designed to extend our technique's utility to plane-wave-based codes. We follow with several illustrative examples of how NBO can be used to elucidate bonding and reactivity in several increasingly sophisticated example systems, including bulk Si, $\alpha$-quartz, the Si(001) dimer reconstruction, and CO adsorption on Pd(111). The latter allows us to directly explore reactive systems of relevance to heterogeneous catalysis via the "chemical" NBO framework.

## II. THEORY

We initially assume that the underlying electronic structure calculation has been carried out in an atom-centered basis and discuss the extension of NBO to periodic systems; we defer the generalization to delocalized plane-wave basis sets until later. We will use the notation of Kudin and Scuseria for all real space orbitals and periodic matrix representations.[41,42]

Beginning with a set of atom centered, atomic orbital (AO) basis functions, $\{\phi_\mu(r)\}$, we generate the corresponding crystalline AOs. For a particular point in the first Brillouin zone, *k*, such an orbital can be represented as

$$\Phi_\mu(k) = \sum_l \mathrm{e}^{ikl}\, \phi_\mu(r - r_\mu - l) \tag{1}$$

where $l$ is a vector to the origin of some unit cell relative to a "central" unit cell with $l = 0$ and $\phi_\mu$ is the periodic image of a basis function in the unit cell indexed by $l$. Thus, $\Phi_\mu(k)$ corresponds to a summation over all real space periodic images of a particular orbital with a *k*-point dependent phase factor.

At each *k*-point, the self-consistent field (SCF) or Kohn−Sham equations are solved by the underlying electronic structure code to obtain a density matrix, $\mathbf{P}^k$, unique to that *k*-point; this density matrix (in the atom-centered basis) is taken directly from the electronic structure code. The density matrix is then transformed into real space values via an inverse Fourier transform:

$$\mathbf{P}^{0l} = \int \mathrm{d}k\, \mathbf{P}^k\, \mathrm{e}^{-ikl} \tag{2}$$

Here, $\mathbf{P}^{0l}_{\mu\nu}$ represents the density matrix element between basis function $\mu$ in the "central" unit cell 0 and basis function $\nu$ in unit cell $l$. Due to locality, it is sufficient to employ some cutoff, $l_{\max}$, such that $\mathbf{P}^{0l_{\max}}_{\mu\nu} \approx 0$. Due to translational symmetry, $\mathbf{P}^{0l} = \mathbf{P}^{h(h+l)}$.

To perform the NBO algorithm, the density matrix, $\mathbf{P}^k$, and overlap matrix, $\mathbf{S}^k$, are obtained in the original AO basis directly from the underlying electronic structure code on whatever *k*-point grid was utilized in the SCF calculation. Using a multistep procedure described in detail elsewhere,[43] we obtain the natural atomic orbitals (NAOs). The NAOs correspond to the linear transform of the AOs resulting in maximally occupied orbitals on each atom, within the molecular environment. As a practical matter, this AO-to-NAO transformation is performed in reciprocal space at each *k* point independently since the necessary symmetric orthogonalizations are time-consuming to implement in real space. While the procedure involves multiple transformations on portions of the density matrix,[43] the overall linear transformation can be represented by a single matrix, $\mathbf{R}^k$. This transformation is then utilized to obtain the density matrix into the NAO basis:

$$\mathbf{P}^{k,\mathrm{NAO}} = \mathbf{R}^k \mathbf{P}^{k,\mathrm{AO}} [\mathbf{R}^k]^\dagger \tag{3}$$

and can be similarly applied to any matrix quantity in the AO basis. An inverse Fourier transform, as in eq 2, is performed on $\mathbf{P}^{k,\mathrm{NAO}}$ to obtain the desired real space representation, $\mathbf{P}^{0l,\mathrm{NAO}}$. The occupancies of the NAO orbitals, the diagonal elements of $\mathbf{P}^{00,\mathrm{NAO}}$, provide a robust population analysis that is rapidly convergent with respect to the choice of basis set.[43]

**II.1. Standard NBO Search.** Prior to discussing the generalization of the NBO search to periodic systems, we briefly review the details of the standard (nonperiodic) NBO search. A comprehensive discussion of this process can be

found elsewhere.[2] First the main diagonal "atomic" blocks of the density matrix corresponding to an individual atomic center A, $\mathbf{P}^{(A)} = \mathbf{P}^{NAO}_{AA}$, are diagonalized to test for eigenvalues above some determined occupancy threshold, generally close to 2. The presence of such a high-occupancy eigenvalue indicates the presence of a one-center bond, $\Omega^{(A)}$, i.e., a lone pair. The combined lone pair density is projected from the density matrix, and the residual matrix is denoted as $\tilde{\mathbf{P}}^{NAO}$. The projection operator, $\mathcal{P}_{A,LP} = \mathbf{I} - |\Omega^{(A)}\rangle\langle\Omega^{(A)}|$, where $\mathbf{I}$ is the identity matrix, is constructed individually for each lone pair orbital found, and the projection is performed on the atomic block.

$$\tilde{\mathbf{P}}^{NAO}_{AA} = \mathcal{P}_{A,LP}\mathbf{P}^{NAO}_{AA}\mathcal{P}_{A,LP} \tag{4}$$

Thus, for each NBO, the appropriate atomic block is found, the NBO density is projected out, and the depleted subblock, $\tilde{\mathbf{P}}^{NAO}_{AA}$, is then returned to the full density matrix.

The NBO search is then extended to two-center bonds via two-atom blocks of the (projected) density matrix,

$$\mathbf{P}^{(AB)} = \begin{bmatrix} \tilde{\mathbf{P}}^{NAO}_{AA} & \tilde{\mathbf{P}}^{NAO}_{AB} \\ \tilde{\mathbf{P}}^{NAO}_{BA} & \tilde{\mathbf{P}}^{NAO}_{BB} \end{bmatrix} \tag{5}$$

with eigenvalues exceeding a predetermined threshold (again near 2) indicating the presence of a potential localized two-center bond. The corresponding eigenvector describing this potential NBO, $\Omega^{(AB)}$, can be further decomposed into two hybrid orbitals, $\Omega^{(AB)} = c_A h^{(AB)} + c_B h^{B(A)}$, where $h^{A(B)}$ is a hybrid orbital centered on atom A (composed solely of NAOs on A) and directed toward atom B.

The complete set of nonbonding lone pairs and potential bonding hybrids on each center are then symmetrically orthogonalized (preventing double-use of any particular NAO), yielding a set of orthonormal hybrid orbitals. Each two-atom density matrix sub-block, $\mathbf{P}^{(AB)}$, can then be transformed into a $(2 \times 2)$ matrix in the hybrid basis of a particular bond. The eigenvalues of this matrix are then tested against a two-center bonding threshold, again close to 2, indicating an NBO composed of an in-phase linear combination of two bonding hybrids. The orthogonal, out-of-phase combination of hybrids yields the corresponding antibonding NBO. The bonding NBOs are then projected out of the density matrix in the same process as for lone pairs, this time restricted to the subspace of the two centers of the bond.

In a system which is perfectly described by one-center lone pairs and two-center bonds, the residual density matrix is formally 0. However, for realistic molecular systems, some residual Rydberg density typically remains. The one-center atomic blocks of the residual $\tilde{\mathbf{P}}^{NAO}$ are diagonalized, yielding the Rydberg orbitals. In most systems, the occupancy of these Rydberg orbitals is minimal, and they merely serve to extend the span of the NBO basis to the full subspace of the AO basis.

**II.2. Periodic Search.** In generalizing to periodic boundary conditions, several changes must be implemented. In the one-center lone pair search, we now search over $\mathbf{P}^{(A)} = \mathbf{P}^{00,NAO}_{AA}$, i.e., the atomic blocks in the central unit cell (which are equivalent to those in other units cells via translational symmetry). In forming two-center blocks, the periodic boundary conditions must be taken into account. The sub-blocks for atom A in the central unit cell and B in unit cell $l$ (which may or may not be the central cell) are constructed as

$$\mathbf{P}^{(AB)} = \begin{bmatrix} \tilde{\mathbf{P}}^{00,NAO}_{AA} & \tilde{\mathbf{P}}^{0l,NAO}_{AB} \\ \tilde{\mathbf{P}}^{l0,NAO}_{BA} & \tilde{\mathbf{P}}^{ll,NAO}_{BB} \end{bmatrix} = \begin{bmatrix} \tilde{\mathbf{P}}^{00,NAO}_{AA} & \tilde{\mathbf{P}}^{0l,NAO}_{AB} \\ \tilde{\mathbf{P}}^{0(-l),NAO}_{BA} & \tilde{\mathbf{P}}^{00,NAO}_{BB} \end{bmatrix} \tag{6}$$

Due to locality, the search for bonds typically covers only the central and nearest neighbor unit cells. To locate all symmetry-unique two-center bonds, the search across two-atom sub-blocks is performed by selecting an atom, A, in the central unit cell and searching across all images of atom B in all unit cells, $l$, for eigenvalues above a set bond occupancy threshold. Then, the next atom is selected in the central unit cell, and the search is repeated for all atoms except those that have already been set as the central unit cell atom, since the bond between atom A in unit cell 0 and atom B in unit cell $l$ is translationally equivalent to the bond between atom A in unit cell $-l$ and atom B in unit cell 0.

Rydberg orbitals are constructed in the same manner as the molecular case, using $\tilde{\mathbf{P}}^{00,NAO}_{AA}$; however, the lone pair and bond NBO density must first be projected out of the NAO density matrix. For a lone pair NBO, this is done in the same fashion as for the molecular case described in section II.1. Even though two-center orbitals are now capable of spanning unit cells, the projector is still straightforwardly constructed as $\mathcal{P}_{AB} = \mathbf{I} - |\Omega^{(AB)}\rangle\langle\Omega^{(AB)}|$, where $\mathbf{I}$ is the identity matrix and $|\Omega^{(AB)}\rangle$ is the two-center NBO as a vector in the NAO basis of centers A and B. The projection is then performed as

$$\tilde{\mathbf{P}}^{(AB)} = \mathcal{P}_{AB}\mathbf{P}^{(AB)}\mathcal{P}_{AB} \tag{7}$$

where $\mathbf{P}^{(AB)}$ is defined in eq 6 and $\tilde{\mathbf{P}}^{(AB)}$ has the exact same sub-block structure, only now depleted of the contribution of $|\Omega^{(AB)}\rangle$.

Note that, by construction, the results of our periodic NBO analysis are invariant to the size of the unit cell. As such, analysis of a supercell yields *identical* results to those of the smaller unit cell so long as commensurate $k$-point samplings are utilized in the underlying electronic structure calculation.

**II.3. Extension to Plane-Wave Basis Sets.** To briefly summarize the developments thus far: we start with a standard periodic electronic structure calculation in an AO basis to obtain the density, $\mathbf{P}^k$, and overlap, $\mathbf{S}^k$, matrices. A set of NBOs, consisting of one-center lone pairs, two-center bonds, antibonds, and Rydberg orbitals are constructed, yielding a Lewis-like picture of localized chemical bonding. Deviations from this perspective can be quantified via interactions between high occupancy one- or two-center orbitals (donors) and low occupancy antibonding/Rydberg orbitals (acceptors) as described in Appendix A. All developments so far can be applied to the output of any atom centered *AO-based* periodic calculation.

To extend the applicability and utility of our NBO procedure beyond calculations performed with atom-centered basis sets, and to PW DFT in particular, we employ a technique for the projection of PW bands into AO basis sets. A similar projection was originally proposed by Sánchez-Portal et al.[44,45] as a means to test the completeness of AO basis sets by comparison to PW results. This technique has also been employed to perform Mulliken population analysis of bulk materials.[46] The projection operator, $\mathcal{P}(k)$, is given by:

$$\mathcal{P}(k) = \sum_{\mu} |\Phi_{\mu}(k)\rangle\langle\Phi^{\mu}(k)| = \sum_{\mu\nu} |\Phi_{\mu}(k)\rangle[S^{k}_{\mu\nu}]^{-1}\langle\Phi_{\nu}(k)| \tag{8}$$

where $|\Phi^{\mu}(k)\rangle$ is the orthogonal dual of the crystalline orbital $|\Phi_{\mu}(k)\rangle$,[47] such that

$$\langle\Phi_{\mu}(k)|\Phi^{\nu}(k)\rangle = \langle\Phi^{\mu}(k)|\Phi_{\nu}(k)\rangle = \delta_{\mu\nu} \tag{9}$$

The completeness of a projection can be quantified using a spillage parameter, $\mathcal{Y}$,

$$\mathcal{Y} = \frac{1}{N_k}\frac{1}{N_\alpha}\sum_{k}^{N_k}\sum_{\alpha}^{N_\alpha}\langle\psi_{\alpha}(k)|(1 - \mathbf{P}(k))|\psi_{\alpha}(k)\rangle \tag{10}$$

Here, $|\psi_{\alpha}(k)\rangle$ is band $\alpha$ in the plane-wave basis, and $N_k$ and $N_\alpha$ are the total numbers of $k$ points and bands, respectively. The spillage can be understood as the average amount of density lost per band during the projection. In the absence of complications (such as non-norm-conserving pseudopotentials, *vide infra*), the spillage parameter is rigorously bounded by 0 and 1, with a spillage of 0 corresponding to a perfect projection.

Due to the incompleteness of the AO basis, the projected bands, $|\chi_{\alpha}(k)\rangle = \mathcal{P}(k)|\psi_{\alpha}(k)\rangle = \sum_{\mu} b_{\alpha,\mu}|\Phi_{\mu}(k)\rangle$, are no longer rigorously orthonormal. This makes the construction of a density matrix in the projected AO basis nontrivial. We apply an occupancy weighted symmetric orthogonalization[43,48] (OWSO) to the projected bands. This orthogonalization generates the set of bands

$$|\chi'_{\alpha}(k)\rangle = \sum_{\mu} b'_{\alpha,\mu}|\Phi_{\mu}(k)\rangle \tag{11}$$

which satisfy the requirement

$$\sum_{\alpha} \mathrm{occ}(\alpha)\| \chi'_{\alpha} - \chi_{\alpha} \|^2 = \text{minimum} \tag{12}$$

where $\mathrm{occ}(\alpha)$ is the occupancy of PW band $\alpha$. This represents the set of orthonormal bands closest to the original set, placing a preference on preserving the original character of higher occupancy bands at the expense of unoccupied bands, which do not enter into the density matrix. The construction of the density matrix from this newly orthogonalized set of bands is then straightforward:

$$\mathbf{P}^{k}_{\mu\nu} = \sum_{\alpha} \mathrm{occ}(\alpha)\, b'_{\alpha,\mu} b'^{*}_{\alpha,\nu} \tag{13}$$

where $\mathrm{occ}(\alpha)$ is again the occupancy of the band in the PW basis. Even though there has been a slight mixing of the bands in the OWSO process, as long as the projection is of a high quality, characterized by a low spillage parameter, the nonorthogonality should be minimal, and therefore little mixing will occur. As such, the occupancy is well-defined. Additionally, the OWSO procedure minimizes the mixing of occupied bands, which are the only ones used in constructing the density matrix. The OWSO also renormalizes the projected bands so that each represents the correct number of electrons according to the original PW band occupancy. As long as the projection is of a high quality, this rescaling remains a small correction.

The use of pseudopotentials (PPs) to describe electrons within the core region around the nucleus is ubiquitous in PW calculations, allowing the highly nodal character of orbitals within the core region to be replaced with a smoother function that can be fully described with a moderate number of PWs. In the projection of Sánchez-Portal et al.,[44,45] norm-conserving PPs were used such that the number of electrons represented by the valence PWs in the core region remains the same as for the all-electron atom. In contrast, most modern PP calculations make use of either ultrasoft or projector augmented-wave (PAW) PPs for increased efficiency and/or accuracy.[49,50] In this case, the number of electrons represented by the PW orbitals in the core region can differ from the real system. As such, the wave function described by the PW basis does not correspond to the "true" (Kohn−Sham) wave function. Rather, for PAW PPs, the true Kohn−Sham wave function, $|\psi_{\alpha,k}(r)\rangle$, for band $\alpha$ at $k$ is given by

$$|\psi_{\alpha,k}(r)\rangle = |\tilde{\psi}_{\alpha,k}(r)\rangle + \sum_{i}(|w_i(r)\rangle - |\tilde{w}_i(r)\rangle)c_{\alpha,i} \tag{14}$$

where $|\tilde{\psi}_{\alpha,k}(r)\rangle$ is the pseudo-wave function in the PW basis. The function $|w_i(r)\rangle$ is the wave function of the real atom within the core region for a particular angular momentum channel and ionic center, collectively indexed by $i$, while $|\tilde{w}_i(r)\rangle$ is the corresponding pseudo-wave function that the optimized PWs mimic. Outside of the core region, these functions are the same, and the correction is zero. The coefficients $c_{\alpha,i}$, come from the SCF results to replace the core region of the PW pseudized wave function based on the character of the band around each atomic center. The difference of these functions, $|\Delta w_i(r)\rangle = |w_i(r)\rangle - |\tilde{w}_i(r)\rangle$, forms the correction that must be included in the projection into the AO basis.

We project both the pseudo-wave function, $|\tilde{\psi}_{\alpha,k}(r)\rangle$, and correction term, $|\Delta w_i(r)\rangle$, using the projector $\mathcal{P}(k)$ of eq 8, and the results are summed together to obtain the projection of the true wave function. Since the projection takes place in reciprocal space, the overlap integrals must be calculated between atomic orbitals and augmenters across unit cells:

$$\langle\Phi_{\mu}(k)|\Delta w_i(k)\rangle = \sum_{l} \mathrm{e}^{-ikl}\langle\phi_{\mu}(r - r_{\mu} - l)|\Delta w_i(r - r_i)\rangle \tag{15}$$

The augmenter functions used in this study have the general form $\Delta w_i(\vec{r}) = R(r - r_i)Y_l^m(\theta,\phi)$, with the radial function, $R(r - r_i)$, represented numerically on a one-dimensional grid, multiplied by an appropriate spherical harmonic, $Y_l^m(\theta,\phi)$. Thus, an analytical expression for the overlap integral necessary for projection is impossible. We thus approximate the real space overlap of the AO and the augmenter correction in two different manners depending on whether the AO and augmenter are for the same atomic center (on-site) or two different centers (off-site). Since standard Gaussian-type AO basis functions have the form $\phi_{\mu}(r) = g(r - r_{\mu})Y_l^m(\theta,\phi)$, the on-site overlap can be reduced to a one-dimensional numerical integral

$$\begin{aligned}\langle\phi_{\mu}(r)|\Delta w_i(r)\rangle &= \langle Y_{l_\mu}^{m_\mu} g(r - r_i)|Y_{l_i}^{m_i} R(r - r_i)\rangle \\ &= \delta_{l_\mu l_i}\delta_{m_\mu m_i}\langle g(r)|R(r)\rangle\end{aligned} \tag{16}$$

Off-site overlaps are more complex. As the augmenter (and thus the overlap) is zero outside of the core region, we expand the AO basis function into a first-order Taylor series about the center of the augmenter function,

$$\begin{aligned}\phi_{\mu}(r - r_{\mu} - l) \simeq{}& \phi_{\mu}(r_i - r_{\mu} - l) \\ &+ \nabla\phi_{\mu}(r_i - r_{\mu} - l)\cdot(\vec{r} - \vec{r}_i)\end{aligned} \tag{17}$$

where $r_i$ is the location of the center on which the augmenter function is located. Since the core region is small and the AOs are smoothly varying far from their respective atomic center, the character of the AO basis function within this region is well approximated. This is functionally an expansion in spherical harmonics to the first order ($l$ = 0, 1) around the augmenter center. Within this approximation, the radial and angular portions are again separable, and terms in the expansion will only have nonzero overlap with augmenter corrections of the same order spherical harmonic (s type with the zeroth order term and $p_j$ type with the corresponding $j$-component of the first order term, e.g. $p_x$ and $\nabla_x\phi_\mu$). Since the oscillatory nature of the augmenter functions increases with higher angular momentum spherical harmonics, this is an excellent approximation. Note, however, that due to these approximations, the spillage will no longer be rigorously bounded, although deviations are in practice small.

It should also be noted that these projection developments are not limited to our periodic NBO implementation but instead allow for any *chemical* analysis technique, which requires bands in an atom-centered basis, to be applied to PW DFT results. This projection technique only requires a fraction of the time of the underlying PW DFT calculation. For example, the projection of the PW bands for the CO on Pd system (*vide infra*) takes only ∼1% of the computer time required for completion of the corresponding PW SCF. Thus, this projection algorithm serves as a very useful tool to interface PW electronic structure codes with analysis techniques that require atom centered basis sets.

## III. COMPUTATIONAL DETAILS

All plane-wave DFT calculations were performed using the Vienna ab initio simulations package (VASP),[51−54] version 4.6. Unless otherwise noted, all calculations utilized PAW pseudopotentials from the VASP database,[49,50] in conjunction with the PBE density functional.[55,56] The default plane-wave cutoff energy of the associated pseudopotential was used, and the SCF was converged to within $10^{-6}$ eV. In all cases, the Brillouin zone was sampled with a Γ-centered Monkhorst-Pack grid.[57] A threshold of at most 0.01 eV/Å for each atom was used for all structural minimizations. All periodic NBO analyses were conducted using our own, original, implementation of NBO, although it is our intention to integrate these developments into the standard NBO distribution in the future. All orbital visualizations were prepared using VMD.[58]

All Gaussian-type atom centered basis sets (utilized for projection, *vide infra*) were trimmed of any functions with angular momentum $l \geq 3$ (f states and higher). None of the systems studied have valence f states, and spillage was found to be minimal without these higher order functions. Even though PPs were utilized for all calculations, core basis functions were still included in the projection. Their inclusion was found to cause a nontrivial decrease in spillage.

## IV. RESULTS AND DISCUSSION

We apply the periodic NBO approach to a variety of representative bulk materials and surface models. These examples serve both to validate the method (comparing bulk NBO results against representative cluster models) and illustrate the utility of the NBO analysis in the context of solid state chemistry and heterogeneous catalysis.

**IV.1. Bulk Silicon.** Bulk silicon serves as a simple test case since it is a prototypical network covalent solid. As such, the "correct" NBO results are trivial to anticipate based on chemical intuition. The cubic diamond unit cell was used, and a 5 × 5 × 5 $k$-point gird was used for Brillouin zone sampling. The lattice constant was allowed to relax to the lowest energy, 5.475 Å. To verify that the projection from a PW to atom-centered basis adequately represents PW density and to probe basis set dependencies, calculations were performed using a norm-conserving PP from the VASP database[59] (to ensure a rigorously bound spillage) utilizing the PW91 density functional.[60,61] Results were projected into various basis sets: the 3-21G family of double-ζ Pople style basis sets,[62−64] the correlation consistent Dunning style basis sets,[65] and a basis set specifically optimized for bulk silicon.[66]

As seen in Table 1, large AO basis sets are *not* required to adequately capture the density represented by the PW bands;

**Table 1. Spillage for Projections into Various Atom-Centered Basis Sets of Bulk Silicon**

| basis set | spillage (%) |
|---|---|
| 3-21G | 1.54 |
| 3-21G(d) | 0.20 |
| 3-21++G | 1.03 |
| 3-21++G(d) | 0.13 |
| cc-pVDZ | 0.22 |
| cc-pVTZ | 0.050 |
| cc-pVQZ | 0.027 |
| cc-pV5Z | 0.019 |
| ref 66 | 0.29 |

even the modest 3-21G basis only fails to capture ∼1.5% of the PW density. The addition of polarization functions decreases the spillage by roughly an order of magnitude, while diffuse functions do little to improve the quality of the projected bands (likely since bulk systems have no "edges" where diffuse functions would be essential). In fact, inclusion of overly diffuse functions creates linear dependencies in the basis set, which lead to numerical instability in calculating $[S^k]^{-1}$, necessary for the projection. We use singular value decomposition to minimize these instabilities and maintain a well behaved projection operator. Similar issues arise when performing SCF calculations for bulk systems with AO basis sets,[66] and guidelines used in selecting basis sets for those calculations should be applied in selecting an appropriate basis set for projection. The final basis set[66] was specifically optimized for use in bulk systems. This is a polarized triple-ζ basis set with less diffuse valence orbitals than isolated atoms.

NBO results for a bulk silicon unit cell, containing eight atoms, reveal a set of 16 symmetry equivalent bonds between $sp^3$ hybrids with all AO basis sets and density functionals, one between each pair of Si nearest neighbors. Searching for bonds that span unit cells (as in eq 6) is necessary to identify nine of these bonds. For the bulk basis set, each bond has an occupancy of 1.92$e$, with a corresponding antibond occupancy of 0.06$e$, and lacks polarization toward either atom, as expected by symmetry. These NBO results are consistent with chemical intuition, confirming the tetrahedrally coordinated, $sp^3$ hybridized, fully covalent bonding that would be expected for this network solid.

We compare our periodic NBO results on bulk silicon to a related hydrogen-capped silicon nanoparticle ($Si_{44}H_{42}$). The

nanoparticle is "carved" from the bulk with Si−Si bonds frozen at bulk distances. This allows us to utilize and compare with standard (molecular) NBO on results obtained from a conventional AO SCF calculation at the same level of theory. The nanoparticle was constructed so that all neighbors of a central Si−Si bond were nonsurface Si atoms. Additional Si atoms were added, so that no surface atom had more than two dangling bonds. Hydrogen atoms were used to cap all dangling bonds and complete tetrahedral coordination. The hydrogen atoms were allowed to relax, and traditional NBO analysis was performed on calculations using Gaussian 09,[67] with the PBE functional[55,56] and bulk basis set.[66] Only interior bonds between silicon atoms each bound to only other silicon atoms were compared to those found in the bulk sample, since other atoms in the cluster are likely influenced by surface effects. All hybrids display $sp^3$ hybridization, and all bonds are nonpolar with an average occupancy of 1.9*e* (although variations of approximately 0.1*e* occur among the Si−Si bonds within the cluster). Note that some variation between bulk and cluster results is expected to arise due to the difference in the underlying electronic structure calculations (e.g., all-electron vs pseudopotential).

**IV.2. Bulk $SiO_2$.** Bulk $SiO_2$ provides an opportunity to evaluate our NBO implementation's capacity to account for ionic bonding in bulk materials, as predicted by the large electronegativity difference ($\Delta\chi$ = 1.9) between Si and O. The $\alpha$-quartz structure[68] consists of silicon atoms tetrahedrally coordinated to oxygen atoms, with each oxygen atom shared between two silicon tetrahedra. PW calculations were performed using a 5 × 5 × 5 *k*-point grid. AO basis sets specifically optimized for bulk silicon[66] and oxide oxygen[69] were used for the projection.

The NAO population analysis shows each O with a charge of −1.18*e* and each Si with +2.36*e*, confirming the expectation of significant ionic character. With one- and two-center occupancy thresholds set to 1.8*e* (reasonable for covalent systems), NBO analysis reveals two lone pairs on each oxygen atom and equivalent bonds between all silicon−oxygen pairs, as shown in Table 2.

**Table 2. Covalent $SiO_2$ NBOs**

| NBO | occupancy | center (bond % polarization) | hybridization (function, %) |
|---|---|---|---|
| Si−O $\sigma$ | 1.967 | Si (15) | s 40, p 60 |
| | | O (85) | s 25, p 75 |
| Si−O $\sigma$* | 0.112 | Si (85) | s 40, p 60 |
| | | O (15) | s 25, p 75 |
| O LP(1) | 1.884 | O (100) | s 0, p 100 |
| O LP(2) | 1.901 | O (100) | s 16, p 84 |

NBO analysis thus suggests a predominantly (although not exclusively) covalent picture of Si−O bonding in silica. The p-type oxygen lone pair is oriented perpendicular to the plane containing the Si−O bonds, while the lone pair with partial s character bisects the O−Si−O angle with the majority of the density situated on the reflex angle side of the oxygen. All bonding NBOs have an almost ideal occupancy, 1.97*e*, indicating that this single Lewis structure should be a good representation of the complete density. However, note that each Si−O bond is highly polarized toward the oxygen atom and that the associated Si−O antibonds are nontrivially occupied at 0.11*e*. As such, the bonds resemble isolated orbitals on the two atoms, with diminished interatomic density. The antibond occupancy, donated from oxygen lone pairs, has been identified as hyperconjugation in siloxane molecular systems,[70] but those authors also suggest that an alternate fully "ionic" Lewis structure may be appropriate for the bulk system. A resonance mixture of these two states would provide the most accurate representation of the density matrix and could be achieved by a natural resonance theory (NRT) analysis.[71−73] This is further evidenced by the original population analysis: the Si charge of +2.36*e* is intermediate between the extreme cases of 0 (purely covalent) and +4 (purely ionic), indicating polar covalent bonding.

**IV.3. Si(001) (2 × 1) Reconstruction.** The Si(001) surface is known to undergo reconstruction via the formation of surface dimers, each with $c(2 \times 1)$ symmetry.[74−78] Since each surface atom at the nonreconstructed surface possesses two dangling bonds, a dimer reconstruction has the potential for $\pi$ bonding.[79] Molecular analogues ($R_2SiSiR_2$) with doubly coordinated silicon atoms adopt a trans-bent structure, with one set of R above the plane of the Si−Si bond while the others shift below.[80] This molecular structure precludes the formation of a traditional $\pi$ bond and arises due to the weakness of Si $\pi$ bonds relative to higher p-hybridization in $\sigma$ bonds and pyramidalization of Si centers.[80,81] However, the presence of bulk coordination below the surface atoms forces a cis-bent orientation of the R groups for the surface dimer (see Figure 1A). With this orientation, a strained, yet $\pi$-like, bond is possible.

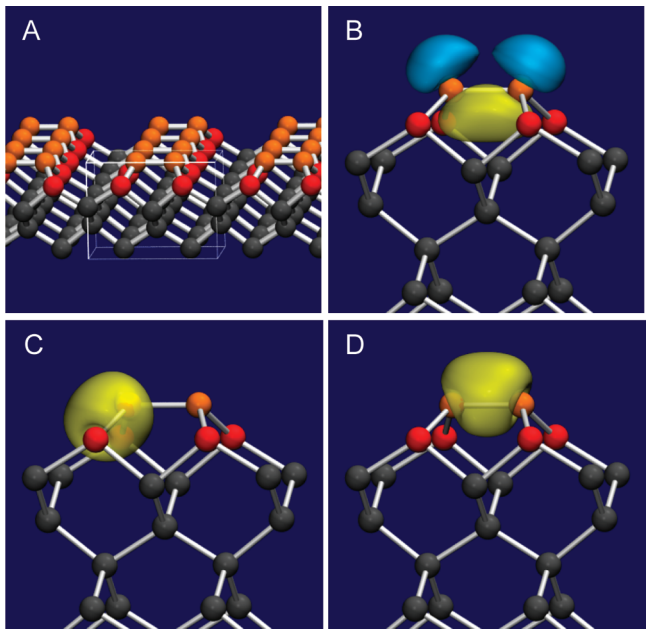


**Figure 1.** Si(001) reconstruction. Orange denotes silicon atoms forming a dimer, red are nearest neighbor silicon atoms, and gray are bulk atoms. (A) The bulk structure with the surface unit cell; (B) dimer $\pi$ bond; (C) neighbor $\sigma$ bond; (D) dimer $\sigma$ bond.

The model surface was constructed starting with the relaxed bulk structure. A $c(2 \times 1)$ surface supercell was constructed from a 10-layer slab of silicon in the *c* direction with a vacuum gap of ∼10 Å. All atoms were allowed to relax freely, and a 7 × 5 × 1 *k*-point grid was utilized. The same bulk silicon AO basis set described above was used for projection.[66]

The bonds of the reconstructed dimer are shown in Figure 1B–D and summarized in Table 3. The observed hybridizations and bond visualizations show a system of two atoms with strained $\sigma$-bonding $sp^2$ hybrids and a $\pi$ bond largely localized *below* the dimer axis. As expected, all Si–Si $\sigma$ bonds have occupancies above 1.9*e*, reflecting silicon's network covalent character. The occupancy of the $\pi$ bond is only 1.49*e*, consistent with the visibly strained bonding orbital. In this highly strained system, the expected lobe *above* the $\sigma$ bond axis is replaced by two largely independent orbitals with negligible overlap, while the lobe *below* the axis exhibits strong overlap. Note that while this is the first NBO analysis of a purely periodic (e.g., bulk) Si(001) surface, Gordon and Tejerina examined a cluster model containing a single dimer unit with qualitatively similar results.[82]

**Table 3. Si(001) Reconstruction NBOs**

| NBO | occupancy | center (bond % contribution) | hybridization (function, %) |
|---|---|---|---|
| dimer $\sigma$ | 1.907 | Si(1) (50) | s 32, p 68 |
| | | Si(2) (50) | s 32, p 68 |
| dimer $\pi$ | 1.490 | Si(1) (50) | s 1, p 99 |
| | | Si(2) (50) | s 1, p 99 |
| dimer $\pi^*$ | 0.410 | Si(1) (50) | s 1, p 99 |
| | | Si(2) (50) | s 1, p 99 |
| neighbor $\sigma$ | 1.914 | Si(1) (49) | s 34, p 66 |
| | | Si(3) (51) | s 24, p 76 |

In this study, the symmetric dimer structure is modeled with the bond axis oriented parallel to the surface plane.[74,75] Buckled structures, where the bond axis is tilted relative to the surface as in the trans-bent molecular structure, have also been proposed.[76−78] There is also the possibility of dynamic buckling, where the dimers oscillate between the two buckled structures and resolve experimentally as an averaged symmetric structure.[74,78] The symmetric structure used here most likely represents an average picture of the reconstruction and captures the nature of dimer bonding. NBO analysis provides a clear and chemically intuitive description of the bonding in the reconstructed dimer, consistent with the classical interpretation.[79]

**IV.4. CO on Pd(111).** Dissociation of CO over metal surfaces is a fundamental catalytic process involved in a host of industrially relevant reactions.[83−86] NBO analysis allows for identification of the specific local interaction(s) responsible for catalytic activity. A comprehensive study of such a reaction might examine configurations along the reaction path, including the transition state, to elucidate the role of the catalyst in terms of transition state stabilization and/or reactant destabilization. NBO analysis could specifically identify the role of catalyst substrate, reactant(s), support and/or promoter species, both individually and synergistically, on reaction activity and product selectivity, thus allowing for the informed synthesis of novel catalysts with specially tuned properties. Here, we take a simpler approach, examining a snapshot of CO adsorption on the Pd(111) surface.

Using the PW91 functional,[60,61] the bulk Pd lattice parameter was obtained by scanning over volume using an 11 × 11 × 11 *k*-point sampling grid, finding a minimum energy at 3.955 Å. A (2 × 2) supercell of the (111) surface was then constructed using six Pd layers and a vacuum gap of 9.2 Å. The bottom three layers were kept frozen in their bulk lattice positions. The surface was allowed to relax, and a CO molecule was then placed onto the top surface. The C atom was positioned directly above a palladium atom, and the C–O bond was oriented perpendicular to the surface, consistent with the experimentally observed top adsorption site. The carbon monoxide and surface were then allowed to relax while using a 5 × 5 × 1 *k*-point grid. A conventional 3-21G basis set was utilized for the AO projection, with the most diffuse s and p orbitals removed from the Pd basis set.[87,88]

The delocalized bonding expected in metals is not well described via the one- and two-center bonding interactions to which our NBO implementation is currently limited. Since we are primarily interested here in only the metal-adsorbate and intra-adsorbate bonding, we choose the utilitarian solution of simply localizing all metal electron density into lone pairs. Note that while metal–metal interactions are effectively "ignored" during the NBO search, they are fully accounted for in the underlying DFT calculations and continue to influence the NBO results via the density matrix. For the case of Pd, five lone pairs, all of pure d character, are found on each center except the adsorbing atom, which lacks a $d_{z^2}$ lone pair (*vide infra*). The lowest occupancy among the lone pairs is 1.72*e* in the bulk and 1.71*e* at the surface. These are relatively high occupancies, consistent with a picture of localized d bands, albeit an incomplete picture. A more rigorous approach would be to extend the capabilities of our bond search to multicenter bonding, similar to AdNDP,[19] which has been shown to capture four-center bonding in fcc-type metal nanoparticles.[23]

The Pd–C and C–O NBOs are featured in Figure 2A–D, with details given in Table 4. The C and O $\sigma$ and $\pi$ bonds are largely unperturbed from those in the isolated molecule, with occupancies of 1.98 and 1.99*e*, respectively. The adsorption bond is therefore formed almost solely from the carbon lone pair of the isolated molecule. The local populations are more drastically affected. In the isolated molecule, the carbon has a charge of +0.41*e*, while at the surface it has +0.67*e*, likely due to the conversion of the fully localized lone pair into a shared C–Pd adsorption bond. The adsorbing palladium atom has a

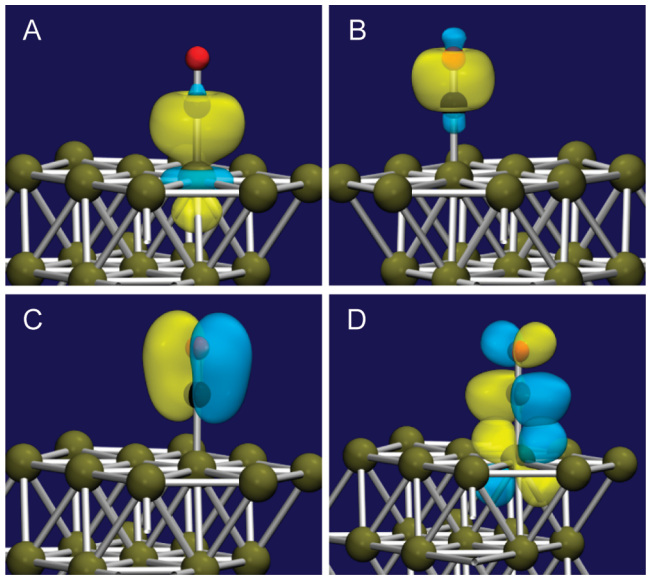


**Figure 2.** NBOs of CO adsoprtion on Pd(111). (A) Pd–C $\sigma$ bond; (B) C–O $\sigma$ bond; (C) C–O $\pi$ bond; (D) Pd lone pair and C–O $\pi^*$ bond.

**Table 4. NBOs of CO adsorption of Pd(111)**

| NBO | occupancy | center (bond % contribution) | hybridization (function, %) |
|---|---|---|---|
| Pd−C $\sigma$ | 1.980 | C (53) | s 63, p 37 |
| | | Pd(47) | s 12, p 11, d 78 |
| Pd−C $\sigma$* | 0.524 | C (47) | s 63, p 37 |
| | | Pd(53) | s 12, p 11, d 78 |
| C−O $\sigma$ | 1.992 | C(31) | s 38, p 62 |
| | | O(69) | s 43, p 57 |
| C−O $\sigma$* | 0.019 | C(69) | s 38, p 62 |
| | | O(31) | s 43, p 57 |
| C−O $\pi$ | 1.991 | C(28) | p 100 |
| | | O(72) | p 100 |
| C−O $\pi$* | 0.202 | C(72) | p 100 |
| | | O(28) | p 100 |
| Pd $d_{xz}$ LP | 1.810 | Pd(100) | d 100 |
| Pd $d_{yz}$ LP | 1.810 | Pd(100) | d 100 |

charge of −0.37*e*, with +0.05*e* on each of the six neighboring surface palladium atoms. No other palladium atom has a charge larger than |0.03|*e*.

The Pd−C bond (Figure 2A) occupancy of 1.98*e* is consistent with the picture of a localized two-center bond, showing that such adsorption interactions can be effectively captured in NBO. The Pd-centered hybrid is largely composed of the $d_{z^2}$ orbital, with contributions from the $p_z$ and s orbitals, entirely consistent with what would arise from symmetry considerations and/or a projected density of states. Nonetheless, it arises in a natural and chemically intuitive manner in NBO analysis and can easily be applied to more complex catalytic systems where symmetry considerations would be less straightforward. Additionally, the 0.52*e* occupancy of the Pd−C antibond hints at a richer picture of adsorption, indicative of the dative nature of the $\sigma$-type adsorbate interaction.

Crucially, we find a 0.20*e* occupancy in each of the $\pi$* C−O orbitals. This nontrivial antibond occupancy demonstrates the electronic contribution to the catalytic activity of the palladium surface; with the lowered C−O bond order, the dissociation barrier decreases. Donor/acceptor analysis (see Appendix A) identifies the source of this antibond occupancy as lone pairs on the adsorbing Pd, as might be expected. As seen in Figure 2D, the predominant sources are from the $d_{xz}$ and $d_{yz}$ lone pairs on the adsorbing Pd atom, consistent with symmetry considerations. These lone pairs have lobes pointing up from the palladium surface with the same symmetry as the $\pi$ orbitals. This is a visual representation of the well-known concept of metal back bonding.[32,89] We anticipate that this $\pi$* NBO occupancy could be used as a possible "descriptor" for use in screening the potential activity of various solid surfaces for C−O dissociation.

## V. CONCLUSION

NBO analysis provides a straightforward and computationally efficient methodology to decompose complex quantum mechanical results into a chemically intuitive representation. Here, we have extended this methodology to systems with periodic symmetry and (via a projection algorithm) PW DFT calculations, opening up a wide area of potential applications. Our periodic NBO method yields results that are directly comparable to those for isolated molecules. As such, it provides a *localized* perspective of bonding and reactivity that is complementary with popular existing analysis approaches for bulk materials such as projected density of states, density differences, etc. Furthermore, NBO's rigorous connection to the density matrix guarantees robust and physically motivated results.

We demonstrate the utility of this approach via a selection of simple model systems. In many of these examples, the bonding and reactivity of these systems has already been interpreted in chemical terms, either on the basis of "chemical intuition" or by complex interpretation of experimental and/or computational data. Nonetheless, these interpretations come out in a rigorous and far more straightforward way from the NBO analysis, providing a direct connection to the underlying electronic structure calculation. Here, our extension of NBO to PW DFT fills an important gap in current analysis methodologies, providing a localized and "chemical" perspective on bonding and reactivity that has been lacking for periodic systems. We are currently working to integrate the periodic NBO approach with a variety of common PW DFT packages and with the standard NBO distribution and anticipate a wide variety of applications in solid state chemistry and catalysis.

## APPENDIX A

### Donor/Acceptor Analysis

The one-center lone pairs and two-center bonds from NBO analysis present an accurate representation of chemical bonding for a stable molecular species, corresponding to a single Lewis structure. The deficiency of the Lewis-type NBOs (bonds and lone pairs) in representing the density matrix can be quantified via the occupancy of these NBOs; the further the occupancy is below 2, the worse the localized picture at representing the true electron density of the system. This non-ideal occupancy corresponds to delocalizations from the Lewis-type orbitals into non-Lewis-type (anti-bonds and Rydberg orbitals), which can be modeled as donor/acceptor interactions using second order perturbation theory.[3] The energy of the delocalization, $\Delta E_{ij}$, is calculated as

$$\Delta E_{ij} = q_i \frac{F_{ij}^2}{\varepsilon_j - \varepsilon_i} \tag{18}$$

where $q_i$ is the occupancy of the donating (Lewis-type) orbital, $\varepsilon_i$ and $\varepsilon_j$ are the energies of the donating and accepting orbitals, and $F_{ij}$ is the off-diagonal element of the Fock matrix in the NBO basis.

To accommodate the translational symmetry, for each Lewis-type NBO, the energy of delocalization is calculated into all periodic images of each non-Lewis-type NBO in each surrounding unit cell in addition to the central unit cell, thus generating a complete set of delocalizing interactions.

## AUTHOR INFORMATION

### Corresponding Author

*E-mail: schmidt@chem.wisc.edu.

### Notes

The authors declare no competing financial interest.

## ACKNOWLEDGMENTS

The authors thank Frank Weinhold and Eric Glendening for many helpful discussions, in particular relating to subtle implementation details of the existing NBO algorithm. Acknowledgment is made to the donors of The American Chemical Society Petroleum Research Fund for partial support

of this research. This work was also funded in part by the Wisconsin Alumni Research Foundation.

## REFERENCES

(1) Weinhold, F.; Landis, C. R. *Valency and Bonding: A Natural Bond Orbital Donor-Acceptor Perspective*; Cambridge University Press: Cambridge, U.K., 2005.
(2) Foster, J. P.; Weinhold, F. *J. Am. Chem. Soc.* **1980**, *102*, 7211−7218.
(3) Reed, A. E.; Curtiss, L. A.; Weinhold, F. *Chem. Rev.* **1988**, *88*, 899−926.
(4) Reed, A. E.; Weinhold, F. *J. Chem. Phys.* **1985**, *83*, 1736−1740.
(5) Carpenter, J. E.; Weinhold, F. *J. Am. Chem. Soc.* **1988**, *110*, 368−372.
(6) Bartlett, G. J.; Choudhary, A.; Raines, R. T.; Woolfson, D. N. *Nat. Chem. Biol.* **2010**, *6*, 615−620.
(7) Alabugin, I. V. *J. Org. Chem.* **2000**, *65*, 3910−3919.
(8) Alabugin, I. V.; Manoharan, M.; Buck, M.; Clark, R. J. *THEOCHEM* **2007**, *813*, 21−27.
(9) Andruniow, T.; Jaworska, M.; Lodowski, P.; Zgierski, M. Z.; Dreos, R.; Randaccio, L.; Kozlowski, P. M. *J. Chem. Phys.* **2008**, 129.
(10) Ben Said, R.; Tangour, B.; Barthelat, J. C. *THEOCHEM* **2008**, *857*, 115−122.
(11) Zhao, L. M.; Wang, Y.; Guo, W. Y.; Shan, H. H.; Lu, X. Q.; Yang, T. *J. Phys. Chem. A* **2008**, *112*, 5676−5683.
(12) Yang, Z.; Rannulu, N. S.; Chu, Y.; Rodgers, M. T. *J. Phys. Chem. A* **2008**, *112*, 388−401.
(13) Pakiari, A. H.; Jamshidi, Z. *J. Phys. Chem. A* **2008**, *112*, 7969−7975.
(14) Sung, C. Y.; Broadbelt, L. J.; Snurr, R. Q. *Catal. Today* **2008**, *136*, 64−75.
(15) Wannakao, S.; Khongpracha, P.; Limtrakul, J. *J. Phys. Chem. A* **2011**, *115*, 12486−12492.
(16) Yung, M. M.; Jablonski, W. S.; Magrini-Bair, K. A. *Energy Fuels* **2009**, *23*, 1874−1887.
(17) Zhou, C. H.; Xia, X.; Lin, C. X.; Tong, D. S.; Beltramini, J. *Chem. Soc. Rev.* **2011**, *40*, 5588−5617.
(18) Subramani, V.; Gangwal, S. K. *Energy Fuels* **2008**, *22*, 814−839.
(19) Zubarev, D. Y.; Boldyrev, A. I. *Phys. Chem. Chem. Phys.* **2008**, *10*, 5207−5217.
(20) Zubarev, D. Y.; Boldyrev, A. I. *J. Org. Chem.* **2008**, *73*, 9251−9258.
(21) Sergeeva, A. P.; Boldyrev, A. I. *Phys. Chem. Chem. Phys.* **2010**, *12*, 12050−12054.
(22) Sergeeva, A. P.; Averkiev, B. B.; Boldyrev, A. I. In *Metal-Metal Bonding*; Parkin, G., Ed.; Springer: Berlin/Heidleberg, 2010; Vol. *136*, pp 275−305.
(23) Zubarev, D. Y.; Boldyrev, A. I. *J. Phys. Chem. A* **2009**, *113*, 866−868.
(24) Ashcroft, N. W.; Mermin, N. D. *Solid State Physics*; Holt: New York, 1976.
(25) Payne, M. C.; Teter, M. P.; Allan, D. C.; Arias, T. A.; Joannopoulos, J. D. *Rev. Mod. Phys.* **1992**, *64*, 1045−1097.
(26) Hafner, J. *J. Comput. Chem.* **2008**, *29*, 2044−2078.
(27) Marzari, N.; Vanderbilt, D. *Phys. Rev. B* **1997**, *56*, 12847−12865.
(28) Souza, I.; Marzari, N.; Vanderbilt, C. *Phys. Rev. B* **2001**, *65*, 035109.
(29) Handgraaf, J. W.; Meijer, E. J. *J. Am. Chem. Soc.* **2007**, *129*, 3099−3103.
(30) Zipoli, F.; Bernasconi, M.; Laio, A. *ChemPhysChem* **2005**, *6*, 1772−1775.
(31) Mugnai, M.; Cardini, G. *J. Chem. Phys.* **2004**, *120*, 5327−5333.
(32) Hoffmann, R. *Solids and Surfaces: A Chemist's View of Bonding in Extended Structures*; VCH Publishers: New York, 1988.
(33) Hughbanks, T.; Hoffmann, R. *J. Am. Chem. Soc.* **1983**, *105*, 3528−3537.
(34) Dronskowski, R.; Blochl, P. E. *J. Phys. Chem.* **1993**, *97*, 8617−8624.
(35) Landrum, G. A.; Dronskowski, R. *Angew. Chem., Int. Ed.* **2000**, *39*, 1560−1585.
(36) Deringer, V. L.; Tchougreeff, A. L.; Dronskowski, R. *J. Phys. Chem. A* **2011**, *115*, 5461−5466.
(37) Bader, R. F. W. *Acc. Chem. Res.* **1985**, *18*, 9−15.
(38) Bader, R. F. W. *Atoms in Molecules: A Quantum Theory*; Clarendon Press: Oxford, U. K., 1990.
(39) Aray, Y.; Rodriguez, J.; Vega, D. In *The Quantum Theory of Atoms in Molecules: From Solid State to DNA and Drug Design*; Matta, C. F., Boyd, R. J., Eds.; Wiley-VCH: Weinheim, Germany, 2007; pp 231−256.
(40) Luana, V.; Blanco, M. A.; Costales, A.; Maori-Sanchez, P.; Martin Pendas, A. In *The Quantum Theory of Atoms in Molecules: From Solid State to DNA and Drug Design*; Matta, C. F., Boyd, R. J., Eds.; Wiley-VCH: Weinheim, Germany, 2007; pp 207−230.
(41) Kudin, K. N.; Scuseria, G. E. *Chem. Phys. Lett.* **1998**, *289*, 611−616.
(42) Kudin, K. N.; Scuseria, G. E. *Phys. Rev. B* **2000**, *61*, 16440−16453.
(43) Reed, A. E.; Weinstock, R. B.; Weinhold, F. *J. Chem. Phys.* **1985**, *83*, 735−746.
(44) Sanchez-Portal, D.; Artacho, E.; Soler, J. M. *Solid State Commun.* **1995**, *95*, 685−690.
(45) Sanchez-Portal, D.; Artacho, E.; Soler, J. M. *J. Phys.: Condens. Matter* **1996**, *8*, 3859−3880.
(46) Segall, M. D.; Shah, R.; Pickard, C. J.; Payne, M. C. *Phys. Rev. B* **1996**, *54*, 16317−16320.
(47) Artacho, E.; Delbosch, L. M. *Phys. Rev. A* **1991**, *43*, 5770−5777.
(48) Carlson, B. C.; Keller, J. M. *Phys. Rev.* **1957**, *105*, 102−103.
(49) Blochl, P. E. *Phys. Rev. B* **1994**, *50*, 17953−17979.
(50) Kresse, G.; Joubert, D. *Phys. Rev. B* **1999**, *59*, 1758−1775.
(51) Kresse, G.; Hafner, J. *Phys. Rev. B* **1993**, *47*, 558−561.
(52) Kresse, G.; Hafner, J. *Phys. Rev. B* **1994**, *49*, 14251−14269.
(53) Kresse, G.; Furthmuller, J. *Phys. Rev. B* **1996**, *54*, 11169−11186.
(54) Kresse, G.; Furthmuller, J. *Comput. Mater. Sci.* **1996**, *6*, 15−50.
(55) Perdew, J. P.; Burke, K.; Ernzerhof, M. *Phys. Rev. Lett.* **1996**, *77*, 3865−3868.
(56) Perdew, J. P.; Burke, K.; Ernzerhof, M. *Phys. Rev. Lett.* **1997**, *78*, 1396−1396.
(57) Monkhorst, H. J.; Pack, J. D. *Phys. Rev. B* **1976**, *13*, 5188−5192.
(58) Humphrey, W.; Dalke, A.; Schulten, K. *J. Mol. Graphics Modell.* **1996**, *14*, 33−&.
(59) Kresse, G.; Hafner, J. *J. Phys.: Condens. Matter* **1994**, *6*, 8245−8257.
(60) Perdew, J. P.; Chevary, J. A.; Vosko, S. H.; Jackson, K. A.; Pederson, M. R.; Singh, D. J.; Fiolhais, C. *Phys. Rev. B* **1992**, *46*, 6671−6687.
(61) Perdew, J. P.; Chevary, J. A.; Vosko, S. H.; Jackson, K. A.; Pederson, M. R.; Singh, D. J.; Fiolhais, C. *Phys. Rev. B* **1993**, *48*, 4978−4978.
(62) Gordon, M. S.; Binkley, J. S.; Pople, J. A.; Pietro, W. J.; Hehre, W. J. *J. Am. Chem. Soc.* **1982**, *104*, 2797−2803.
(63) Pietro, W. J.; Francl, M. M.; Hehre, W. J.; Defrees, D. J.; Pople, J. A.; Binkley, J. S. *J. Am. Chem. Soc.* **1982**, *104*, 5039−5048.
(64) Clark, T.; Chandrasekhar, J.; Spitznagel, G. W.; Schleyer, P. V. *J. Comput. Chem.* **1983**, *4*, 294−301.
(65) Woon, D. E.; Dunning, T. H. *J. Chem. Phys.* **1993**, *98*, 1358−1371.
(66) Porter, A. R.; Towler, M. D.; Needs, R. J. *Phys. Rev. B* **1999**, *60*, 13534−13546.
(67) Frisch, M. J.; Trucks, G. W.; Schlegel, H. B.; Scuseria, G. E.; Robb, M. A.; Cheeseman, J. R.; Scalmani, G.; Barone, M.; Mennucci, B.; Petersson, G. A.; Nakatsuji, H.; Caricato, M.; Li, X.; Hratchian, H. P.; Izmaylov, A. F.; Bloino, J.; Zheng, G.; Sonnenberg, J. L.; Hada, M.; Ehara, M.; Toyota, K.; Fukuda, R.; Hasegawa, J.; Ishida, M.; Nakajima, T.; Honda, Y.; Kitao, O.; Nakai, H.; Vreven, T.; Montgomery, J. A., Jr.; Peralta, J. E.; Ogliaro, F.; Bearpark, M.; Heyd, J. J.; Brothers, E.; Kudin, K. N.; Staroverov, V. N.; Kobayashi, R.; Normand, J.; Raghavachari, K.; Rendell, A.; Burant, J. C.; Iyengar, S. S.; Tomasi, J.; Cossi, M.; Rega,

N.; Millam, J. M.; Klene, M.; Knox, J. E.; Cross, J. B.; Bakken, V.; Adamo, C.; Jaramillo, J.; Gomperts, R.; Stratmann, R. E.; Yazyev, O.; Austin, A. J.; Cammi, R.; Pomelli, C.; Ochterski, J. W.; Martin, R. L.; Morokuma, K.; Zakrzewski, V. G.; Voth, G. A.; Salvador, P.; Dannenberg, J. J.; Dapprich, S.; Daniels, A. D.; Farkas, O.; Foresman, J. B.; Ortiz, J. V.; Cioslowski, J.; Fox, D. J. *Gaussian 09*, revision A.02; Gaussian, Inc.: Wallingford, CT, 2009.
(68) Lepage, Y.; Donnay, G. *Acta Crystallogr., Sect. B: Struct. Sci.* **1976**, *32*, 2456−2459.
(69) Dovesi, R.; Roetti, C.; Freyriafava, C.; Apra, E.; Saunders, V. R.; Harrison, N. M. *Philos. Trans. R. Soc. London, Ser. A* **1992**, *341*, 203−210.
(70) Weinhold, F.; West, R. *Organometallics* **2011**, *30*, 5815−5824.
(71) Glendening, E. D.; Weinhold, F. *J. Comput. Chem.* **1998**, *19*, 593−609.
(72) Glendening, E. D.; Weinhold, F. *J. Comput. Chem.* **1998**, *19*, 610−627.
(73) Glendening, E. D.; Badenhoop, J. K.; Weinhold, F. *J. Comput. Chem.* **1998**, *19*, 628−646.
(74) Hamers, R. J.; Tromp, R. M.; Demuth, J. E. *Phys. Rev. B* **1986**, *34*, 5343−5357.
(75) Tromp, R. M.; Hamers, R. J.; Demuth, J. E. *Phys. Rev. Lett.* **1985**, *55*, 1303−1306.
(76) Chadi, D. J. *Phys. Rev. Lett.* **1979**, *43*, 43−47.
(77) Yang, C.; Kang, H. C. *J. Chem. Phys.* **1999**, *110*, 11029−11037.
(78) Dabrowski, J.; Scheffler, M. *Appl. Surf. Sci.* **1992**, *56*−*8*, 15−19.
(79) Hamers, R. J.; Avouris, P.; Bozso, F. *Phys. Rev. Lett.* **1987**, *59*, 2071−2074.
(80) Trinquier, G.; Malrieu, J. P. *J. Phys. Chem.* **1990**, *94*, 6184−6196.
(81) Pauling, L. *Proc. Natl. Acad. Sci. U. S. A.* **1983**, *80*, 3871−3872.
(82) Tejerina, B.; Gordon, M. S. *J. Phys. Chem. C* **2008**, *112*, 754−761.
(83) Schulz, H. *Appl. Catal., A* **1999**, *186*, 3−12.
(84) Hu, P.; King, D. A.; Lee, M. H.; Payne, M. C. *Chem. Phys. Lett.* **1995**, *246*, 73−78.
(85) Liu, Z. P.; Hu, P. *J. Chem. Phys.* **2001**, *114*, 8244−8247.
(86) Inderwildi, O. R.; Jenkins, S. J.; King, D. A. *Angew. Chem., Int. Ed.* **2008**, *47*, 5253−5255.
(87) Binkley, J. S.; Pople, J. A.; Hehre, W. J. *J. Am. Chem. Soc.* **1980**, *102*, 939−947.
(88) Dobbs, K. D.; Hehre, W. J. *J. Comput. Chem.* **1987**, *8*, 880−893.
(89) Blyholder, G. *J. Phys. Chem.* **1964**, *68*, 2772−2777.